

# An Imaging Polarimeter(IMPOL) for multi-wavelength observations

A. N. Ramaprakash<sup>1</sup>, Ranjan Gupta<sup>1</sup>, A. K. Sen<sup>2</sup>, and S. N. Tandon<sup>1</sup>

<sup>1</sup> Inter-University Centre for Astronomy and Astrophysics, Post Bag 4, Ganeshkhind, Pune - 411 007, INDIA

<sup>2</sup> Center for Plasma Physics, Sapta Shwahid Marg, Dispur, Guwahati - 781 006, INDIA

Received; Accepted

**Abstract.** — Taking advantage of the advances in array detector technology, an imaging polarimeter (IMPOL) has been constructed for measuring linear polarization in the wavelength band from 400-800 nm. It makes use of a Wollaston prism as the analyser to measure simultaneously the two orthogonal polarization components that define a Stoke's parameter. An achromatic half-wave plate is used to rotate the plane of polarization with respect to the axis of the analyser so that the second Stoke's parameter also can be determined. With a field of view corresponding to about  $30 \times 30 \text{ mm}^2$  for a  $\text{Ø}1.2 \text{ m}$ ,  $f/13$  telescope, a sensitive, liquid-N<sub>2</sub> cooled CCD camera as the detector and a built-in acquisition and guidance unit, the instrument can be used for studying stellar fields or extended objects with an angular resolution of  $\sim 2''$ . The instrumental polarization is less than 0.05% and the accuracies of measurement are primarily limited by photon noise for typical observations.

**Key words:** instrumentation: polarimeters – techniques: polarimetry – polarization

## 1. Introduction

The advances in two dimensional array detector technology in the optical and near infrared wavelength bands have made new kinds of imaging astronomical observations feasible. Astronomical polarimetry is one field which has gained tremendously from these developments. The limitations of using aperture photometry for polarimetry were so severe that any serious study was rendered time consuming and difficult. On the other hand, imaging polarimetry with its capabilities for multiplexing, simultaneous sky measurement, seeing-limited resolution etc. offer great advantages over aperture polarimetry. Astronomers have recognized this potential and have developed several new observation techniques in the optical (eg. Scarrott 1991; Jannuzi et. al. 1993; Jarrett et. al. 1994; Wolstencroft et. al. 1995; Simmons et. al. 1995) and near infrared (eg. Kastner & Weintraub 1994; Moore & Yamashita 1995; Weintraub et. al. 1995) wavelengths to study phenomena in a variety of Galactic and extragalactic astrophysical objects. In this paper, we report the design and construction of an imaging polarimeter (IMPOL) which uses a cooled CCD array as detector. It was developed at the Inter-University Centre for Astronomy and Astrophysics (IUCAA), INDIA. The principle of the instrument (Sen & Tandon 1994) is based on a combination of ideas sug-

gested by Ohman (1939) and Appenzeller (1967). An instrument of this type has been constructed at the University of Durham and has been in use for some time now (Scarrott et. al. 1983). Section 2 is a description of the instrument – the different subsections dealing with various aspects ranging from design guidelines to instrument control and user-interface. The dominant sources of errors in the measurement are investigated in Sect. 3, while an estimate of the performance of the instrument under two typical observing conditions is given in Sect. 4; Section 4 also contains an estimate of the performance of the acquisition & guidance unit. In Sect. 5 we discuss the observational procedure and the data-analysis method. Section 6 contains results of the commissioning tests of the instrument. The last section (Sect. 7) contains the concluding remarks.

## 2. The Instrument

The following set of scientific and technical guidelines were adopted as basis for the design of the instrument. (i) It should be capable of observing faint extended objects like reflection nebulae, accretion disks, dusty active galaxies etc., with accuracy limited by photon noise and resolution limited by seeing. This demands a typical field of view of a few arcminutes, an optics which is well-matched with the telescope to minimize loss of light and a detec-

tor of sufficient sensitivity. Also, the effects of atmospheric scintillation should be eliminated and instrumental polarization minimized so that such measurements of low level polarization could be made. (ii) Since the objects of interest are very often quite faint, the instrument should have an acquisition and guidance (A&G) system which allows pointing the telescope with an accuracy of a few arcseconds and tracking to better than  $1''$  over long periods. (iii) Multi-wavelength observations should be possible in various wavelength bands in the optical and near-IR regions. (iv) The entire instrument consisting of the optics, A&G unit, associated electronics etc. should be a self-contained unit which can be easily mounted on the telescope, with only electrically isolated communication links to the computers for instrument control and data acquisition. (v) The cost of the instrument should be minimized by using standard optical and electronic components and by avoiding over-specification as far as possible.

### 2.1. Principle of the instrument

Figure 1 is a schematic representation of the optical arrangement of IMPOL. The basic idea behind this arrangement is to use a Wollaston prism with its axis normal to the optical axis of the system, as the analyser to convert the linear polarization in the incoming light into relative intensity of two orthogonally polarized beams (the ordinary and the extraordinary), separated by a small angle of  $0.5^\circ$ . This measurement is sufficient to define one of the Stoke's parameters Q or U. The other Stoke's parameter can be determined by rotating the plane of polarization of the incoming light relative to the analyser through a known angle and taking another measurement. This is accomplished by introducing a half-wave plate, with its fast-axis normal to the optical axis of the system, before the Wollaston prism. When the half-wave plate is rotated through an angle  $\alpha$ , the plane of polarization rotates through an angle  $2\alpha$ . At this new position of the half-wave plate another measurement on the orthogonally polarized beams can be made to determine the second Stoke's parameter as well. It is easily seen that, for this arrangement the intensities of the extraordinary and ordinary beams ( $I_e$  and  $I_o$ ) are given by

$$I_e(\alpha) = \frac{I_{\text{up}}}{2} + I_p \cos^2(\theta - 2\alpha) \quad (1)$$

$$I_o(\alpha) = \frac{I_{\text{up}}}{2} + I_p \sin^2(\theta - 2\alpha), \quad (2)$$

where  $I_{\text{up}}$  &  $I_p$  are the intensities in unpolarized and polarized condition respectively in the incoming beam;  $\theta$  &  $\alpha$  are the position angles of the polarization vector and the half-wave plate fast-axis respectively with reference to the axis of the Wollaston prism. Since the angle  $\theta$  is conventionally measured with respect to the celestial north-south axis (and increasing counter-clockwise), the axis of the Wollaston prism is kept aligned to it. We define the ratio

$$R(\alpha) = \frac{\frac{I_e}{I_o} - 1}{\frac{I_e}{I_o} + 1} = p \cos(2\theta - 4\alpha), \quad (3)$$

where  $p = \frac{I_p}{I_{\text{up}} + I_p}$ , is the fraction of the total light in linearly polarized condition. This ratio reduces to the normalized Stoke's parameters  $\frac{Q}{I}$  and  $\frac{U}{I}$  for  $\alpha = 0^\circ$  and  $\alpha = 22.5^\circ$ . In practice, additional measurements are made at two more values of  $\alpha$ , namely  $45^\circ$  and  $67.5^\circ$ , for reasons explained in Sect. 5.

The half-wave plate and the Wollaston prism are placed in between a field lens-camera lens combination, which reimages the telescope focal plane on to the main CCD with a reduction factor of about 2.7; the field lens reimages the telescope aperture on the half-wave plate and the light reaches the camera lens without any vignetting. As shown in Fig. 1 each point in the telescope focal plane produces two images on the CCD, corresponding to the ordinary and the extraordinary beams. In order to avoid overlap of the images of adjacent points, for observations of extended objects, a grid of parallel obscuring strips is placed at the focal plane of the telescope. The width of and spacing between the strips are chosen in such a way as to avoid the overlap of the ordinary and the extraordinary images on the CCD. Four 0.3 mm diameter holes are provided at the four corners of the grid and are used to focus the surface of the grid, which coincides with the focal plane of the telescope, on to the surface of the CCD. The grid is made of black dielectric material to avoid polarization of the stray light arising due to reflections from its edges. Besides, the edges are made slanted (Fig. 1) to prevent vignetting of the telescope beam.

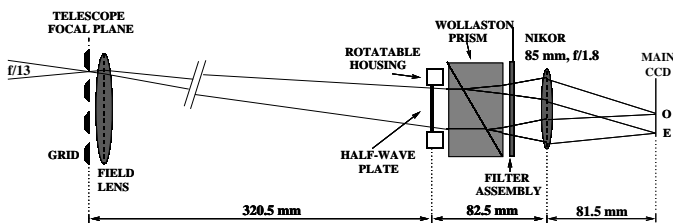


Fig. 1 Schematic of the IMPOL optical layout

### 2.2. Acquisition and Guidance Unit

A schematic illustration of the Acquisition and Guidance (A&G) unit is shown in Fig. 2. The right-angle prism, the field lens (L1) and a relay lens (L2) are held in position inside a probe which in turn is mounted on a linear XY translator stage. This arrangement allows the probe to be positioned anywhere within a  $40 \times 100 \text{ mm}^2$  rectangular area (corresponding to about 45 square minutes of arc for

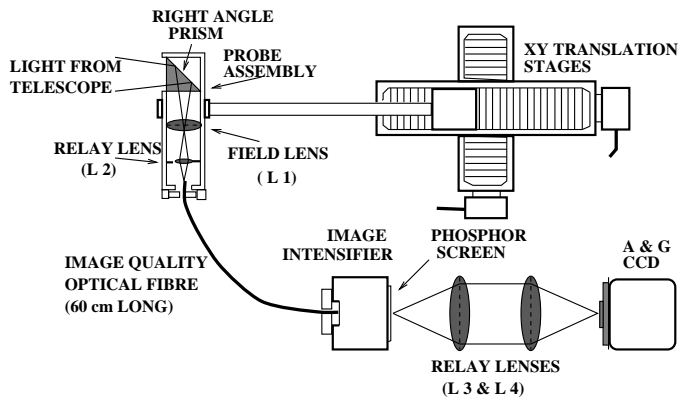


Fig. 2 Schematic of the Acquisition & Guidance unit

a  $\varnothing$ 1.2 m, f/13 telescope) close to the main field. The lens L2 reimages a  $\varnothing$ 12 mm area of the telescope focal plane on to the tip of an image quality optical fibre which, in turn, conveys it to the photocathode of an image intensifier. Two Nikon lenses (L3 and L4) focus the intensifier output on the surface of the CCD of the A&G unit.

For pointing the telescope, atleast one star brighter than about 15<sup>th</sup> mag. in visual and close to the main field is identified and its right ascension and declination values are entered in to the control computer along with those of the main object. Once the translation stages are moved to the requisite offset coordinates by the computer, short exposures are taken with the CCD of the A&G unit to adjust the telescope pointing such that the guide star appears at the center of the CCD. Now the telescope has been pointed and auto-guiding is started. During auto-guiding the control computer takes successive exposures with the CCD and finds the centroid of the guide star image. Error signals are then generated accordingly and transmitted to the control system of the telescope.

Table 1 is a list of the optical components used in IMPOL along with their sources and part numbers. The field lens, half-wave plate, Wollaston prism and the filters were unmounted when purchased.

### 2.3. Instrument control, Data-acquisition and User-interface

A mixture of digital and analogue electronics hardware and a layered architecture software have been used to perform the instrument control and data-acquisition operations. Apart from the control computer (PC 486), all the electronics is mounted on the telescope along with the instrument. The upper three layers of the software reside in the control computer, while the lower two layers are downloaded into the local memory of the instrument at the time of start-up and initialization.

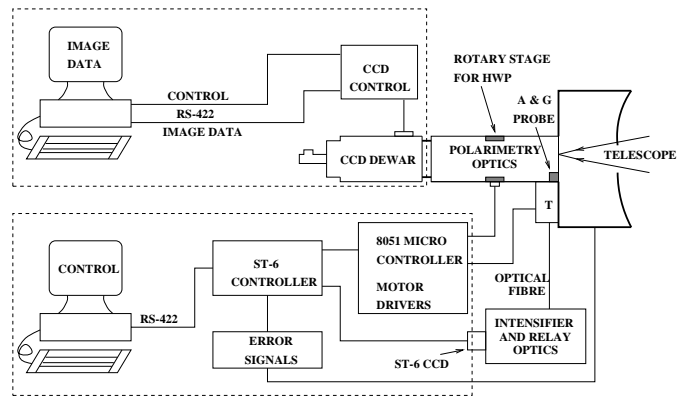


Fig. 3 Various blocks of the IMPOL control system. The block marked “T” represents the XY stages for positioning the probes.

#### 2.3.1. Electronics

The electronics assembly of the instrument consists of three parts - (i) the positioning systems for the half-wave plate and the A&G unit probe, (ii) the CCD camera for the A&G unit and the associated electronics and (iii) the main CCD camera with its own control electronics and host computer (PC 486) for exposure control and data-acquisition. A block schematic of the IMPOL control system is shown in Fig. 3. The half-wave plate and the A&G unit probe are positioned using stepper motors which are controlled with signals generated by a 8051 microcontroller based card. These digital control signals are fed to translator circuits which convert them to power-amplified phase signals required to drive the stepper motors. Sensors are used on the half-wave plate mount and the A&G unit XY positioning stages for fixing the zero positions. The controller card, in turn, receives “command” packets from the computer for instrument control.

The detector for the A&G unit is the commercially available ST-6 CCD camera of the Santa Barbara Instrument Group (SBIG). This camera has a controller unit of its own which executes specific tasks under the command of the control computer. (The SBIG have, in a private communication, graciously provided us the instruction set for their controller which we have used in our custom-software for instrument control.) The “command-response” exchange between the control computer and the instrument takes place over an optically isolated asynchronous serial communication link (RS 422 standard). The ST-6 controller has a second serial communication port (AUX port) so that it can be used as a gateway for communicating with other peripherals which use the same type of communication link. The 8051-based controller card, described above, is connected to this AUX port and the communication between it and the control computer is routed through the ST-6 controller (see Fig. 3).

**Table 1.** Optical components used in IMPOL

Component	Source	Part number	Description
Field lens	Karl Lambrecht	322305	$\varnothing$ 50 mm, eff. FL 300 mm, AR coated, achromat
Half-wave plate	Karl Lambrecht	WPAC 2-22-BB400/700	achromatic, 22 mm clear aperture, broad band single layer AR coated
Wollaston prism	Bernard Halle	PWQ 30.30	quartz, 29x29 mm clear aperture, multi layer AR coated
Filters	Andover		B, V and R, $\varnothing$ 40 mm, 5 mm thick, AR coated, image quality
Camera lens	Nikon		eff. FL 85 mm, f/1.8, A.F.
Right-angle prism	Melles Griot		12x12 mm
Lenses L1	Edmund Scientific		eff. FL 25 mm, f/2.0
L2			eff. FL 6 mm, f/2.0
Optical fibre	Dolan Jenner	ISO 636	6x6 mm, coherent glass fibre, 36 inch long, N.A. 0.66,
Image intensifier	Philips	XX1500	$\varnothing$ 14 mm, resolution 36 lp/mm
Lenses L3 & L4	Nikon		eff. FL 50 mm, f/1.2

The main CCD camera for data-acquisition is built around a liquid N<sub>2</sub> cooled, 385×578 pixel, front-side illuminated, phosphor coated CCD chip from EEV. The operations of the CCD camera like shutter control, binning mode selection etc. are carried out by another 8051-based controller card which communicates with the data-acquisition computer over a second asynchronous serial communication link. Once the exposure is over the image pixel data are transmitted to the computer over a high speed cable using dedicated circuits. The important parameters of this CCD camera, which was also developed at IUCAA, are listed in Table 2 (for more details refer to Deshpande and Gadre 1994).

### 2.3.2. Software

The instrument control software is made of five layers, of which none but the top most one is visible to the user. This layer provides the user-interface, reads the system configuration files and initializes the system. It is at this level where the sequence of operations is decided, depending upon the instructions given by the user and corresponding service calls to the immediate lower level are generated. The second layer provides these services mostly by creating a “command+parameter(s)” packet depending on the service requested and the current system configuration and then passing this packet on to the third software layer. The communication protocol between the control computer and the microcontrollers at the instrument is defined in the third layer which sends the packet to the ST-6 controller or through it to the 8051-based

**Table 2.** The parameters of IUCAA CCD Camera

Parameters	Value
CCD make	EEV CCD02-06 series
CCD chip size	385(H)×578(V)
Pixel size	22 × 22 $\mu$ m
Active area	12.7 mm × 8.5 mm
No. of amplifiers	1
Quantum efficiency	blue : 20% yellow : 50% red : 60%
Readout speed	32 $\mu$ s per pixel
Acquisition & Display time	12 s for full frame
Read noise (total)	8 e <sup>-</sup> rms
Gain	5 e <sup>-</sup> / ADU

controller for positioning operations. Upon receiving a “command+parameter” packet, either of these controllers parses it and checks for errors. If the command is valid and there are no errors it immediately sends back an acknowledgement signal. Otherwise it sends back a corresponding error signal. The result of this communication process is conveyed back to the highest layer for appropriate follow up. It is to be noted that at this stage the top most layer does not have information whether its service request has actually produced the required effect or not. To obtain this information it has to generate another ser-

vice call requesting the current status of the appropriate system parameters.

The 8051 microcontroller has a built-in interpreter for BASIC. The processes of packet reception, parsing, error checking and acknowledging are carried out by a BASIC program which resides in the memory of the microcontroller forming the fourth software layer. A set of assembler routines, each doing a specific operation, forms the fifth and lowermost software layer. The BASIC program calls one of these assembler routines to execute the particular task requested by the command.

This system of control encashes on the fact that while each individual operation is to be carried out fast, the interval between successive operations are comparable to typical user response time scales. Though the layered architecture appears complicated, it is in fact extremely easy to implement and debug and provides great flexibility to alterations.

### 3. Sources of errors

In addition to the fundamental limit due to photon statistics, the measurement of polarization is affected by several factors beginning from the atmosphere down to the detector and the data-analysis procedure. In the following four subsections we look at, in some detail, the important sources of errors and the techniques used to minimize their effects.

#### 3.1. Atmospheric Effects

Since polarization measurement involves taking multiple exposures, variations in atmospheric transparency and scintillations can affect the measurement process. In IMPOL, two orthogonal polarization components are measured simultaneously and the Stoke's parameter is obtained from the ratio of the fluxes in these components (Eq. (2)). Since the atmosphere is not birefringent, this eliminates the effects due to atmospheric scintillation, or for that matter any effect which changes both the polarization components by the same factor—like variations in the effective exposure times of observations, presence of thin clouds etc.

#### 3.2. Distortions in polarization

As the measurements depend on detecting changes in the polarization vector caused by rotating the half-wave plate, any small instrumental polarization occurring after the half-wave plate can be easily eliminated. All the optical elements are anti-reflection coated to minimize the polarization effects due to reflection at their surfaces, and care is taken to minimize the stray light, reflected from the walls etc., reaching the detector. In particular, all the aperture stops in the beam path are chosen to be non-metallic, including the grid in the focal plane, so as to

avoid polarization of light scattered from these (Pospergelis, 1965). The mounts for field lens, the half-wave plate and the Wollaston prism have been designed to minimize stress-birefringence due to differential thermal expansion.

The retardance introduced by the half-wave plate could deviate from  $180^\circ$  either because of the finite angle of incidence or because of the chromatic effects. If the beam is incident at a small angle  $i$ , the maximum change in retardance is given by (derived from expression in Serkowski 1975)

$$\sigma_\tau \simeq \pi \times \frac{i^2}{4n_o} \left( \frac{1}{n_o} - \frac{1}{n_e} \right), \quad (4)$$

where  $n_o$  and  $n_e$  are the refractive indices of the material for ordinary and extraordinary rays. For the aperture used, the maximum angle of incidence is about  $5^\circ$  so that  $\sigma_\tau \lesssim 0.01$  rad. The chromatic effects give  $\sigma_\tau < 0.18$  rad for the wideband and  $\sigma_\tau < 0.14$  rad for the V-band. It can be shown (Serkowski 1974) that the depolarization  $\sigma_p$  due to an uncertainty of  $\sigma_\tau$  rad in the retardance is to the lowest order given by  $\sigma_p \simeq p\sigma_\tau^2$ ,  $p$  being the fractional polarization. Therefore even for the wideband  $\sigma_p \lesssim 0.03p$ . Further, circular polarization in the incident light is converted to a linear polarization of magnitude  $V\sigma_\tau$ , where  $V$  is the circularity parameter. For wideband observations, conversion to linear polarization would be about  $0.18V$ , but in typical observations this does not pose a serious problem because the circular polarization in the incident light is usually less than the linear polarization.

Another chromatic effect is the change in position angle of the half-wave plate fast axis with wavelength. Although this does not produce any error in the measurement of fractional polarization  $p$ , it does render the measurement of position angle  $\theta$  erroneous. A solution to this problem is to observe standard stars using narrow band filters and produce a smoothed curve which gives the required position angle correction for each wavelength. The achromatic half-wave plate used in IMPOL does not produce any appreciable dispersion in its fast-axis position angle over the wavelength range of interest.

The uncertainty involved in the positioning of the half-wave plate leads to an error in the measurement of polarization. From Eq. (2), we can see that a positioning uncertainty of  $\sigma_\alpha$  produces a maximum error in the measurement of linear polarization given by  $\sigma_p \simeq p\sigma_\alpha$ . Thus for an error of  $0.1^\circ$ , of the positioning system, this results in  $\sigma_p \simeq 0.002p$ .

#### 3.3. Flat field errors

The half-wave plate is the only moving component in the optical train and hence it is relatively easy to make sure that the images do not shift on the detector. Further, as the analyser is fixed with respect to the detector, the orientation of the ordinary and extraordinary polarizations also remain fixed with respect to it, independent of the

polarization vector of the incident beam. This renders it easy to estimate the flat field correction factor from the set of observations at the four positions of the half-wave plate. These points are further explained in Sec. 5.

### 3.4. Photon noise

From the above discussion we find that all the sources of errors described do not contribute more than  $0.05p$  to the error in the measurement of  $p$ . In the next section, we estimate the errors under typical observing conditions that result from photon noise alone. Comparing the two, we conclude that the dominant source of error in the typical measurement of polarization is photon noise. From equation (2) it can be shown that the variance due to photon noise in the measurement of each of the Stoke's parameters  $R(\alpha)$  is given by

$$\sigma_R^2 = \frac{4I_o I_e}{(I_o + I_e)^3} (1 + k), \quad (5)$$

where  $I_o$  and  $I_e$  are the number of photoelectrons and  $k$  is the ratio of the flux from the background to that from the source. For small values of  $p$ ,  $I_o$  and  $I_e$  are approximately equal and denoting  $I = I_o + I_e$ , the standard deviation of  $p$  can be written as

$$\sigma_p \simeq 100 \times \frac{\sqrt{I + I_B}}{I} \%, \quad (6)$$

where  $I_B = kI$ . Similarly, we can also show that

$$\sigma_\theta \simeq 0.5 \times \frac{\sigma_p}{p} \text{ rad}. \quad (7)$$

It is worth noting here that  $p$ , as defined above, is a positive definite quantity and follows the Rice probability distribution given by

$$F(p, p_0) = \frac{p}{\sigma_p} e^{-\frac{p^2 + p_0^2}{2\sigma_p^2}} I_0\left(\frac{pp_0}{\sigma_p^2}\right). \quad (8)$$

Here,  $p_0$  is the true value of fractional polarization being estimated by  $p$  and  $I_0$  is the modified Bessel function of order zero. Since  $p$  is a biased estimator, several schemes have been suggested (Simmons & Stewart 1984 and references therein) for debiasing, but none of them is fully satisfactory. For values of  $\frac{p}{\sigma_p}$  larger than about 4, almost all the debiasing schemes agree and reduce approximately to the relation

$$\hat{p}_0 = p \sqrt{1 - \frac{\sigma_p^2}{p^2}}, \quad (9)$$

where  $\hat{p}_0$  is the ‘‘debiased’’ estimate of  $p_0$ . Thus it is desirable to work with the normalized Stoke's parameters as far as possible and use the quantities  $p$  and  $\theta$  only to present the final results. However, in general, the normalized Stoke's parameters themselves might not be normally

distributed and might have bias (Clarke et. al. 1983). Besides, for photon-noise dominated measurements, the positive kurtosis of the distribution will lead to erroneous estimates of the confidence levels unless more than a few thousand photoelectrons are collected. Thus, in order to arrive at an optimum procedure, it is essential to carefully study the nature of the dominant sources of noise in the measurement and their effects on the analysis (see Sec. 5).

## 4. Performance estimates

An estimate of the performance of the instrument is made in the following two sub-sections. In the first part we calculate the accuracy of polarization measurement as limited by photon noise for two typical types of observations. The second part deals with the performance of the A&G unit. In both cases, it is assumed that the observations are made in the V-band (bandwidth  $\Delta\lambda \sim 100$  nm,  $V_0 = 1000$  photons per  $\text{cm}^2$  per s per  $\text{\AA}$ ) using a  $\text{\O}1.2$  m (area  $A \sim 10^4$   $\text{cm}^2$ ) telescope having an f/13 beam, that the brightness of the sky is 20 mag. per sq. arcsec and that the software aperture used for photometry has about 30 pixels, ie. about 30 sq. arcsec.

### 4.1. Polarimetry

In the following discussion the combined effect of the atmosphere, the telescope, the optics and quantum efficiency of the detector etc., is found to result in an effective transmission of  $\eta \sim 3.2\%$ .

A classical example of polarimetric observations involves study of dark molecular clouds with the light of stars shining behind their periphery (eg. Elvius 1970; Joshi et al. 1985; Kane et al. 1995). Such studies give valuable information regarding the properties of dust in the cloud and the magnetic field in its vicinity. Typically the polarization of these sources is in the range 1–5 %. Assuming stars of apparant visual magnitude  $m_v = 15$ , we see that the total number of photo-electrons collected, due to the star ( $I$ ) and the background ( $I_B$ ), within the software aperture, for an exposure of 15 minutes are  $2.9 \times 10^5$  and  $8.6 \times 10^4$  respectively. Therefore, the corresponding error in polarization measurement is given by

$$\sigma_p = 100 \times \frac{\sqrt{2.9 \times 10^5 + 8.6 \times 10^4}}{2.9 \times 10^5} \simeq 0.21\%. \quad (10)$$

If the observations are made with a filter which covers both the V and R bands ( $\Delta\lambda \sim 200$  nm), there will be an improvement in the signal-to-noise ratio by a factor of  $\sqrt{2}$ , giving  $\sigma_p \sim 0.15\%$ .

Study of extended objects like reflection nebulae, is another field in which polarimetric observations are useful. Polarization in the light scattered from these clouds can range from a few percent to as much 30%. Assuming that the observation involves a reflection nebula of the

same surface brightness as the background sky, the integrated photoelectron count from each, for an exposure of 15 minutes, will be  $8.6 \times 10^4$  and hence

$$\sigma_p = 100 \times \frac{\sqrt{8.6 \times 10^4 + 8.6 \times 10^4}}{8.6 \times 10^4} \simeq 0.48\% . \quad (11)$$

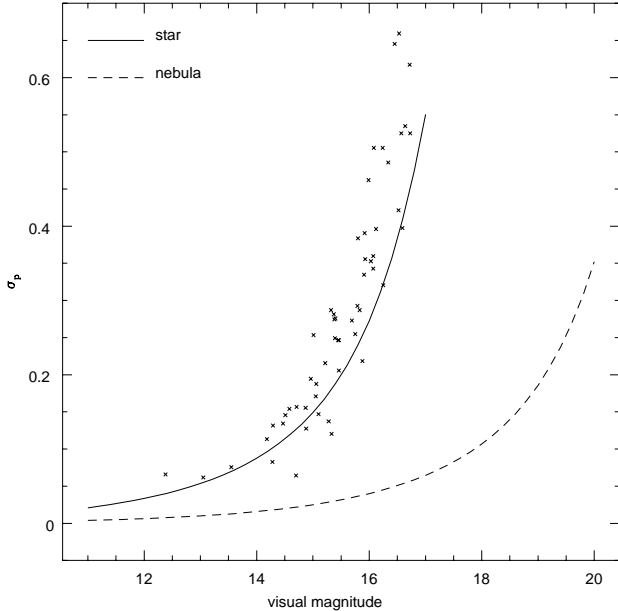


Fig. 4 The errors due to photon noise alone, as calculated in Sec. 4.1, for wideband measurements of fractional polarization  $p$  are shown as a function of the brightness of the source. The solid curve refers to the case of stars while the dashed curve is for an extended object, for which the x-axis represents the surface brightness of the source in magnitudes per sq. arcsecs. The background is assumed to be  $20^{th}$  magnitude per sq. arcsec and a software aperture of 30 sq. arcsec has been used during data reduction. The crosses represent the errors in actual polarimetric measurements made with instrument on a field at the periphery of the dark cloud B133.

for a solid angle defined by the software aperture. The wideband observations, in this case will give an error of about 0.34%.

In Fig. 4 the solid and dashed curves show how the error in the measurement of fractional polarization, based on photon statistics alone, changes as a function of source brightness, for the two cases discussed above, namely stellar sources and reflection nebulae respectively.

#### 4.2. Acquisition & Guidance (A&G) unit

The A&G unit has a field of view of about  $2'$  and can be positioned anywhere within a  $40 \times 100 \text{ mm}^2$  area at the focal plane of the telescope close to the main field. This

area has been chosen on the basis of the requirement that three stars brighter than  $m_v = 15$  should be available with 95% confidence level towards the poles of the Galaxy.

In this case, apart from the atmospheric and telescope transmission losses, account has to be made for losses in the probe optics, optical fibre and the quantum efficiency of the intensifier. Together this amounts to an effective transmission of  $\sim 0.1$ . The gain of the intensifier can be varied from 2000 to 50000 and the effective transmission of the lenses L3 and L4 and the ST-6 CCD is about 3%. Therefore the signal-to-noise ratio remains essentially unchanged in the stages after the intensifier. An exposure of 1 s for a star of  $V \sim 15$  mag., gives a signal-to-noise ratio of about 20 in each of the 10 pixels covered by the image. This is sufficient to obtain an auto-guidance accuracy better than  $0.1''$  with a correction frequency of about a second. However, in order to avoid excessive jitter, hysteresis has been introduced into the system so that the corrections will occur only if a minimum shift of  $0.2''$  has been sensed in the stellar image centroids.

### 5. Observations and Data-analysis

We have seen in Sect. 2.1 that observations for at least two positions of the half-wave plate are required to determine the three unknown parameters namely, the total intensity ( $I$ ), fraction of light in linearly polarized condition ( $p$ ), and position angle of the plane of polarization ( $\theta$ ). However, the situation is not so simple in reality because – (i) the responsivity of the system to the two orthogonal polarization components may not be the same, and (ii) the responsivity of the CCD is a function of the position on its surface. Due to these effects the signals which are actually measured in the two images ( $I'_e$  and  $I'_o$ ) are given by

$$\begin{aligned} I'_e(\alpha) &= I_e(\alpha)F_e(x, y) \quad \text{and} \\ I'_o(\alpha) &= I_o(\alpha)F_o(x, y) , \end{aligned} \quad (12)$$

where  $F_e(x, y)$  and  $F_o(x, y)$  represent the effects mentioned above;  $(x, y)$  being the coordinates on the array surface. If it is ensured that the ordinary and extraordinary images do not move on the surface of the CCD during different exposures, the ratio of the factors  $F_o$  and  $F_e$  can be estimated as

$$\frac{F_o}{F_e} = \left[ \frac{I'_o(0^\circ)}{I'_e(45^\circ)} \times \frac{I'_o(45^\circ)}{I'_e(0^\circ)} \times \frac{I'_o(22.5^\circ)}{I'_e(67.5^\circ)} \times \frac{I'_o(67.5^\circ)}{I'_e(22.5^\circ)} \right]^{\frac{1}{4}} , \quad (13)$$

by making use of the fact that a rotation of the half-wave plate by  $45^\circ$  simply leads to an interchange of the signals in the ordinary and extraordinary images. Now the actual ratio of the fluxes in the two images may be recovered as

$$\frac{I_e(\alpha)}{I_o(\alpha)} = \frac{F_o}{F_e} \times \frac{I'_e(\alpha)}{I'_o(\alpha)} . \quad (14)$$

This ratio is substituted in Eq. (2) and a cosine curve is fitted to the four values of  $R(\alpha)$  obtained so as to make the best estimates of  $p$  and  $\theta$ .

In practice, it might also become necessary to take several exposures at each half-wave plate position so as to collect sufficient number of photons to get the required signal-to-noise ratio. This might also become necessary if there are stars in the field with very large magnitude differences. Then a set of short exposures have to be taken to avoid the bright stellar images from saturating while a set of longer exposures will be required to collect sufficient photons from the fainter stars. In order to ensure that the normalized Stoke's parameters follow a normal distribution as close as possible, the basic observational quantities, namely the fluxes measured at each position of the half-wave plate, should be averaged together before taking their ratios to give the normalized Stoke's parameters. However, this method has its demerits too. Firstly, it leaves the non-linear  $\chi^2$  fitting technique with only one degree of freedom, to estimate the two parameters  $p$  and  $\theta$  from the four values of  $R(\alpha)$ . Secondly, it does not allow the estimation of errors in the measurement of the Stoke's parameters, since there are not enough degrees of freedom. Therefore, it appears optimum to use a fitting technique to estimate  $p$  and  $\theta$ , from the values of  $R(\alpha)$  obtained from individual exposures.

Since a grid of parallel obscuring strips is placed at the telescope focal plane (Sect. 2.1), only less than half the field is seen by the detector during any observation. Once a set of exposures has been taken for all the four positions of the half-wave plate, the telescope orientation is slightly changed so as to see the other part of the field which was previously obscured by the grid strips. Alternatively, in the case of stellar fields with slowly changing (in intensity and polarization) background, the grid may be removed during observations, provided the field is not too crowded.

The images are collected by the data-acquisition computer during observations and later transferred to cartridge tapes. The data analysis is carried out on UNIX-based workstations. A polarimetry package has been developed for this purpose within the IRAF environment using a mixture of standard IRAF tasks, custom-made CL scripts and FORTRAN routines. The images are first subjected to the preliminary steps of bias and dark removal, cosmic ray and bad pixel detection, and masking etc. PSF fitting tasks of the DAOPHOT package are then used to determine accurately the centroids of the stellar images. The intensity estimates are, however made using aperture photometry covering a diameter greater than  $2 \times \text{FWHM}$  so as to integrate more than 90% of the signal. (The FWHM is kept greater than 3 pixels to minimize the effects of undersampling and intrapixel variation of quantum efficiency.)

## 6. Commissioning of IMPOL

The commissioning of the instrument involved two levels of tests. Firstly laboratory tests were conducted on the optical bench to determine the various parameters like linear-

ity, gain and readnoise of the detector, vignetting, depolarization, instrumental polarization etc. Some necessary modifications were made in the optical system and the software in order to optimize the instrument performance. Measurements were made with a 3000 K filament source in B, V, R bands, and a wide band defined by a 3 mm thick KG3 glass. A 100% polarized beam showed that the depolarization is about 0.4% in the B and V bands, less than 1% in the R band, and less than 6% in the broad band. There was no discernible rotation of the position angle between these bands. For R and the wideband, the accuracy of measurements is limited by the performance of the polarizer used. In order to estimate the instrumental polarization, a Lyot depolarizer was introduced in front of the artificial star and the polarization was measured. This experiment showed that the instrumental polarization is about 0.03% in the B-band and less than 0.06% with the wideband filter.

**Table 3.** Observations of standard stars

Star	$p$	$\sigma_p$	$\theta$	$\sigma_\theta$	$\sigma_{\text{phot}}$	$p_0$	$\theta_0$
(1)	(2)	(3)	(4)	(5)	(6)	(7)	(8)
HD	%	%	°	°	%	%	°
43384	3.05	0.04	172	0.3	0.03	3.0	170
154445	3.65	0.03	90.5	0.2	0.02	3.7	90
102870	0.03	0.01	64.4	7.8	0.02	0.017	162
39587	0.03	0.03	140	27.5	0.02	0.013	20
	0.05	0.02	159	12.7	0.02		
	0.09	0.02	34	6.7	0.02		
	0.05	0.02	167	11.3	0.02		

The second stage of tests were conducted when the instrument saw the first light in February 1996, at the  $\text{O}1.2$  m Gurusikhar Infra-Red Telescope facility on Mt. Abu, Rajasthan, operated by the Physical Research Laboratory at Ahmedabad, India. Several standard polarized and unpolarized stars were observed at this time. Since the standard stars are too bright, having visual magnitudes in the range of 4 to 7, instrument was slightly defocused to avoid saturation of pixels in reasonable exposure times.

Table 2 contains the results of the observations in V-band. Column 1 of the table gives the identification number of the star. Columns 2-5 contain the measured values and  $1\sigma$  errors of the fractional polarization  $p$  and the position angle  $\theta$ . Column 6 gives the error  $\sigma_p$  based on photon statistics alone, derived as illustrated in Sect. 3. Cols. 7 and 8 list the published values of  $p$  and  $\theta$ .

The first two stars in the table are polarized standards while the last two are unpolarized ones. Comparing the



measured and published results for the polarized stars we see that there is no indication of depolarization. Neither is there any rotation of the position angle beyond a couple of degrees. From Col. 3 and Col. 6 for the unpolarized stars, we see that the error in the measured polarization is comparable with that expected on the basis of photon statistics alone. In Fig. 5, the values of  $q = R(0^\circ)$  are plotted against  $u = R(22.5^\circ)$  for all the unpolarized standards observed in the V-band. The extremely low correlation coefficient between  $q$  and  $u$ , is indicative of the low instrumental polarization. The average values of  $q$  and  $u$ , give a value of polarization  $p = 0.03\%$ . These observations show that for accuracies  $\lesssim 0.05\%$  in the measurement of polarization  $p$ , the performance is still limited by photon noise and the instrument polarization floor has not yet reached. The four measurements of star HD39587 are made at different corners of the CCD frame in order to verify the uniformity of response.

The data which is required to incorporate the A&G system was also collected during this observation run. The A&G system was successfully installed during a second observation run with the same telescope in late May, 1996. This time, several observations of stellar fields at the periphery of some dark molecular clouds were also made. The analysis of this data is in progress at present and will be reported separately. The accuracy of the polarization measurement can be gauged from the results for some of these stars shown in Fig. 4.

## 7. Conclusion

An Imaging Polarimeter (IMPOL) has been constructed which uses mostly standard optical and electrical components, but through careful design has been able to achieve

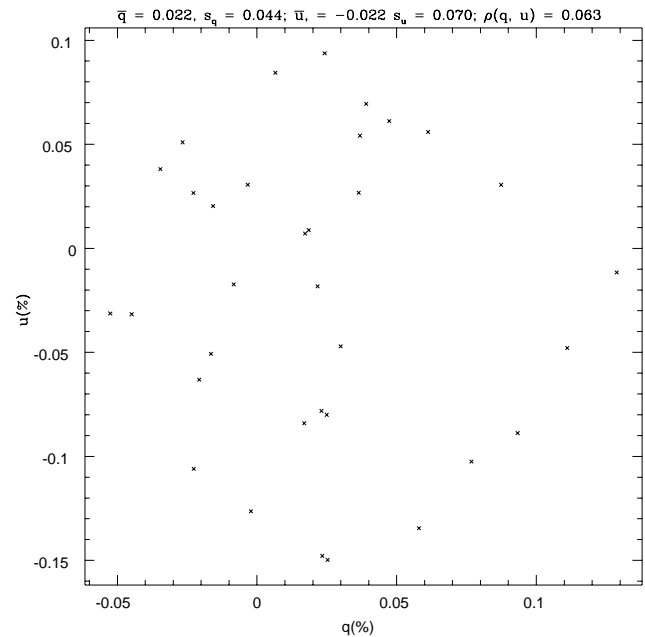


Fig. 5 Normalized Stoke's parameter  $q$  is plotted against  $u$  for a number of unpolarized standard stars. The correlation coefficient of the points is about 0.06 and the average values of  $q$  and  $u$  give a value of  $p = 0.03\%$ .

photon-noise limited performance. The instrument has a field of view of about  $6.5'$  for a  $\text{Ø}1.2$  m,  $f/13$  telescope, and the detector is a sensitive, liquid  $\text{N}_2$  cooled CCD. An off-axis acquisition and guidance unit capable of using stars as faint as  $V_{\text{mag}} \sim 15$  is also built in the instrument so that long exposures of faint extended objects like reflection nebulae etc. can be taken while keeping the image fixed on the CCD face to within one half of a pixel – this stability of the image is a necessary condition to achieve a high accuracy in relative photometry between the different frames used to estimate the polarization. Observations of nearby standard polarized and unpolarized stars show that for wideband observations, there is no discernible depolarization and the instrumental polarization is less than  $0.05\%$ . Preliminary results of wideband polarimetry of stellar fields, using a PSF fitting technique for determining the centroids of the stellar images and aperture photometry with a radius of 3 pixels to derive the intensities of the individual images, give close to photon-noise limited accuracy of  $0.15\%$  for  $V_{\text{mag}} = 15$  stars with about an hour of total exposure time. For extended objects with brightness about 20th mag. per square arcseconds and a background of about the same brightness, it is estimated that an accuracy of about  $1\%$  is possible with 60 minutes of total exposure time and an aperture of 10 sq. arcsec.

*Acknowledgements.* The project has been funded by the Department of Science and Technology of the Government of India. The authors also wish to thank the Physical Re-

search Laboratory, Ahmedabad for providing telescope time, P. A. Chordia and R. Bedade for their involvement in developing the electronic circuitry for the instrument and M. S. Deshpande for her assistance during its commissioning.

## References

- Appenzeller I., 1967, *PASP*, 136
- Clarke D., Stewart B. G., Schwarz H. E., Brooks A., 1983, *A&A*, 126, 260
- Deshpande M. S., Gadre D. V., 1994, in: *Proceedings of the Indo-US Workshop on Array detectors and Image processing*, eds. S. N. Tandon and A. N. Ramaprakash, IUCAA, INDIA, p. 237
- Elvius A., 1970, in: *Dark nebulae, Globules and Protostars*, ed. Lynds B. T. The University of Arizona Press, Tucson, p. 57
- Jannuzi B. T., Smith P. S., Elston R., 1993, *ApJS*, 85, 265
- Jarrett T. H., Novak G., Xie T., Goldsmith P. F., 1994, *ApJ*, 430, 743
- Joshi U. C., Kulkarni P. V., Bhatt H. C., Kulshrestha A. K., Deshpande M. R., 1985, *MNRAS*, 215, 275
- Kane B. D., Clemens D. P., Leach R. W., Barvainis R., 1995, *ApJ*, 445, 269
- Kastner J. H., Weintraub D. A., 1994, *ApJ*, 434, 719
- Moore T. J. T., Yamashita, T., 1995, *ApJ*, 440, 722
- Ohman Y., 1939, *MNRAS*, 99, 624
- Pospergelis M. M., 1965, *SvA-AJ*, 9, 313
- Scarrott S. M., Warren-Smith R. F., Pallister W. S., Axon D. J., Bingham R. G., 1983, *MNRAS*, 204, 1163
- Scarrott S. M., 1991, *Vist. Astron.* 34, 163
- Sen A. K. and Tandon S. N., 1994, in: *Instrumentation in Astronomy VIII*, ed. D. L. Crawford, SPIE proceedings, Vol. 2198, part 1, p. 264
- Serkowski K., 1974, in: *Methods of Experimental Physics: Astrophysics*, eds. N. Carleton, Vol. 12, part A, Academic Press, p. 361
- Serkowski K., 1975, in: *Planets, Stars and Nebulae studied with photopolarimetry*, ed. T. Gehrels, The University of Arizona Press, Tucson, p. 135
- Simmons J. F. L., Willis J. P., Newsam A. M., 1995, *A&A*, 293, L46
- Simmons J. F. L., Stewart B. G., 1984, *A&A*, 142, 100
- Weintraub D. A., Kastner J. H., Whitney B. A., 1995, *ApJ*, 452, L141
- Wolstencroft R. D., Done C.J., Scarrott S. M., Scarrott R. M. J., 1995, *MNRAS*, 276, 460